

## Article

# *Aspergillus terreus*-Mediated Selenium Nanoparticles and Their Antimicrobial and Photocatalytic Activities

Ebrahim Saied <sup>1</sup>, Alsayed E. Mekky <sup>1</sup>, Abdulaziz A. Al-Askar <sup>2</sup>, Abdelrahman F. Hagag <sup>1</sup>, Abdullah A. El-bana <sup>1</sup>, Mohamed Ashraf <sup>1</sup>, Abdelrahman Walid <sup>1</sup>, Taha Nour <sup>1</sup>, Mahmoud M. Fawzi <sup>1</sup>, Amr A. Arishi <sup>3</sup> and Amr H. Hashem <sup>1,\*</sup>

<sup>1</sup> Botany and Microbiology Department, Faculty of Science, Al-Azhar University, Cairo 11884, Egypt

<sup>2</sup> Department of Botany and Microbiology, Faculty of Science, King Saud University, P.O. Box 2455, Riyadh 11451, Saudi Arabia

<sup>3</sup> School of Molecular Sciences, The University of Western Australia, Perth, WA 6009, Australia

\* Correspondence: amr.hosny86@azhar.edu.eg

**Abstract:** Selenium (Se) is a nutritional component necessary for animal and plant development and reproduction. Selenium nanoparticles (SeNPs) have a high absorption rate during routine supplementation. In the current study, a cell-free extract of *Aspergillus terreus* was used as a reducing and stabilizing agent in the synthesis of SeNPs using a green and eco-friendly method. The mycosynthesized SeNPs were characterized by UV-visible spectrophotometry, Fourier transform infrared spectroscopy, X-ray diffraction spectroscopy, dynamic light scattering, transmission electron microscopy, and scanning electron microscopy. The results of the characterization process showed that the mycosynthesized SeNPs had spherical shapes and sizes less than 100 nm. Results showed that mycosynthesized SeNPs exhibited promising antibacterial activity against both Gram-positive and Gram-negative bacteria where inhibition zones were 14, 20, 16, and 13 mm toward *S. haemolyticus*, *S. aureus*, *E. coli*, and *K. pneumoniae*, respectively. However, it had weak antifungal activity against *C. albicans*, where the inhibition zone was 12 mm. The efficacy of mycosynthesized SeNPs for the decolorization of malachite green dye was investigated. Results illustrated that SeNPs exhibited rapid biodegradation of malachite green dye, reaching up to 89% after 240 min. In conclusion, SeNPs were successfully biosynthesized using *A. terreus* and demonstrated both antimicrobial and photocatalytic activities.

**Keywords:** selenium nanoparticles; antimicrobial activity; fungi; biosynthesis and decolorization



**Citation:** Saied, E.; Mekky, A.E.; Al-Askar, A.A.; Hagag, A.F.; El-bana, A.A.; Ashraf, M.; Walid, A.; Nour, T.; Fawzi, M.M.; Arishi, A.A.; et al. *Aspergillus terreus*-Mediated Selenium Nanoparticles and Their Antimicrobial and Photocatalytic Activities. *Crystals* **2023**, *13*, 450. <https://doi.org/10.3390/cryst13030450>

Academic Editors: Abdur Rauf and Mujeeb Ur Rehman

Received: 6 February 2023

Revised: 20 February 2023

Accepted: 26 February 2023

Published: 4 March 2023



**Copyright:** © 2023 by the authors. Licensee MDPI, Basel, Switzerland. This article is an open access article distributed under the terms and conditions of the Creative Commons Attribution (CC BY) license (<https://creativecommons.org/licenses/by/4.0/>).

## 1. Introduction

Water, a significant asset with unique properties, is essential for the survival of living organisms, hydroelectric power generation, industries and conveyance [1]. Rapid industrialization has led to an excessive increase in chemical use, which has gradually increased environmental damage, notably water contamination [2]. Large amounts of pollutants are released into freshwater resources by several enterprises. Large amounts of wastewater, including a variety of biodegradable and non-biodegradable contaminants, are produced by the textile industry [3]. The synthetic dyes used in the coloring process are a major reason for concern among all pollutants since the bulk of the dye is discharged into the effluent and only a very small percentage of the dye binds to the fabric. Every year, approximately  $3 \times 10^8$  kg of dyes are discharged into wastewaters globally [4]. Since azo dyes are the most widely used dyes and the main source of environmental concern due to their complicated structural makeup and resistive character, they affect both people and the environment. Due to the use of dangerous dyes, these industrial effluents have a disastrous impact on aquatic life and people. These dyes are not biodegradable, act as oxidizing agents, are stable to light, are carcinogenic, and are difficult to remove from

wastewater [5,6]. Malachite green is a typical triphenylmethane dye that is widely used in the dyeing industry. However, several studies have shown how it can have teratogenic, mutagenic, and cancerous effects on people [7]. Diverse methods, such as coagulation or flocculation, adsorption, membrane filtration, ultrafiltration, etc., have been used to remove colors from wastewater [8]. Due to its simplicity of use and lack of secondary pollutants, adsorption is the most popular technology among all of them. Malachite green dye has been adsorptively removed from water using a range of materials, including activated carbon, clays, polymers, magnesium oxide, ferric oxide, silica, sawdust, hydrogels, cellulose textiles, and zeolites [9]. These techniques have a number of limitations, including a high level of sludge production, the need for physiochemical monitoring, and the inability to reuse coagulants or flocculants. The usage of adsorbents is further hampered by their high cost, the removal of sludge, recycling, and saturation. Additionally, reverse osmosis has expensive operating and maintenance requirements. A costly membrane filtering system is used in ultrafiltration [10,11].

Significant attention has been given to nanotechnology for environmental remediation, and it has a bright future in improved wastewater treatment and biological treatments [12,13]. Due to their distinct physical and chemical properties, such as their optical, electrical, and catalytic properties, nanoparticles have the potential to function as a catalyst in the oxidation reaction that purifies industrial effluent water. Metallic and semiconductor nanoparticles are useful for the catalytic and photocatalytic breakdown of dyes in aquatic environments [14]. The effectiveness of dye degradation was increased by nanoparticles because of their unique properties and high surface-to-volume ratio [15,16]. The major benefit of this procedure is that no trash or solid hazardous elements are produced. In addition to this biogenic synthesis, nanomaterials have also been produced via a variety of physical and chemical processes [17–22]. When comparing the three synthesis techniques, biological synthesis is more important than physical and chemical synthesis of nanoparticles and more inexpensive, opening the way for a new era of bionanotechnology [23–26]. Recently, biological methods utilizing plants or microorganisms have been made available [17,27–29]. Traditional methods in medical applications do have adverse effects since they require a significant level of hazardous chemical consumption, high heating conditions, expensive equipment, and the adsorption of these toxic chemical compounds on the surface. Green synthesis is promoted as a dependable, easy-to-use, non-toxic, inexpensive, and environmentally responsible method that makes use of naturally existing organisms, microalgae, plants, and enzymes [30–34]. The majority of microorganisms are fungi, which have several uses in a variety of scientific fields, including biofuels, organic acids, food items, nanotechnology, bioremediation, and bio-deinking [35–39]. Numerous studies have been done on the use of metal oxides in heterogeneous catalysis for the degradation of organic dyes [40]. Doping was also thought to improve the catalyst's photocatalytic activity, causing considerable degradation. However, as time passes, a route for selenides becomes available [41]. Se is a semiconductor that is widely used in modern instruments such as electrical or optical devices, photoconductors, and electrodes in the form of binary selenides with transition metals. Se also has unusual physical properties, such as strong optical conductivity, anisotropy in thermal conductivity, and X-ray sensor responses [42]. Se is a micronutrient that is necessary for the manufacture of selenoproteins, which include a number of well-studied selenoenzymes, the majority of which have oxidoreductase activity. Se is also vital for plants and animals [43]. In order to create selenoproteins and selenoenzymes like peroxidases and reductases, the amino acid selenocysteine [44], which is a precursor to Se, must be present. The literature has reported on a number of different metal selenide photocatalysts. SeNPs have excellent biological activity because they are bioavailable, biodegradable, and less harmful to people or animals. Se is a trace element and considered a vital cofactor of antioxidant enzymes [45]. The United Kingdom organization of vitamins and minerals said that men and women should consume 60 and 70 µg of Se daily, respectively. A daily consumption of more than 400 µg may be harmful and result in selenosis, a disorder. Se is a vital biological component of glutathione peroxidase,

an enzyme that functions as an antioxidant by protecting crucial SH-groups and breaking down peroxides. Without the use of reducing and stabilizing chemicals, biogenic Se NPs offer a secure and eco-friendly way for producing metal/metalloid nanoparticles with excellent bioactivity and minimal cytotoxicity [46]. Due to its well-known photoelectrical and semiconducting properties, Se is employed in xerography, rectifiers, solar cells, and photographic exposure metres [47]. The creation of highly efficient and nontoxic antibiotics has become a major research area because bacterial infection poses a severe threat to human health and because bacterial resistance is a result of long-term overuse of high-dose antibiotics. One of the most promising recent methods to combat multidrug resistance is the creation of non-antibiotic materials that make use of nanotechnology. SeNPs have been discovered to exhibit a variety of biological effects, including immunomodulatory effects [48], antibacterial [49], anticancer [50], antioxidant [51], and antidiabetic activity [52]. Se is thought to be healthier and less hazardous to healthy cells than the aforementioned metal-based compounds due to its presence in the human body [53]. The current study aims to myco-synthesize SeNPs by harnessing metabolites of the fungal strain *A. terreus*. Furthermore, it will be tested for antimicrobial and photocatalytic degradation activities.

## 2. Materials and Methods

### 2.1. Materials

All chemicals used in this study, including sodium selenite, the inorganic compound with the formula  $\text{Na}_2\text{SeO}_3$  and sodium hydroxide (NaOH), were of analytical grade and purchased from Sigma-Aldrich, Egypt (purity 99%).  $\text{Na}_2\text{SeO}_3$  was used as a precursor for the synthesis of SeNPs. All cultured media were purchased from HiMedia (Egypt) (purity 99%). All biological syntheses in the current study were achieved using distilled water (dis.  $\text{H}_2\text{O}$ ).

### 2.2. Isolation and Identification of Fungal Isolate

The fungal isolate was isolated from a cultivated soil sample collected from Al-Sharqia Governorate, Egypt (GPS N:  $30^\circ 43' 58.12''$ , E:  $31^\circ 58' 23.15''$ ). For the serial dilution approach, soil samples were used as inoculums and then plated on Martin Rose Bengal Agar medium. The plates were incubated for 4 days at  $28^\circ\text{C}$ . Individual fungal colonies were selected and further purified by sub-culturing on Potato Dextrose Agar (PDA) medium. Following nuclear ribosomal DNA internal transcribed spacer (ITS) sequencing, the fungal isolate was identified using morphological and microscopic observations (such as color, the texture of the mycelia, spore production pattern, etc.). Using accepted procedures, the CTAB extraction technique was used to isolate the genomic DNA. With the assistance of the primers for ITS1 f (5-CTTGGTCATTTAGAGGAAGTAA-3) and ITS4 (5-TCCCTCCGCTTATTGATATGC-3), a fungal internal transcribed spacer (ITS) rDNA region was amplified. The PCR-amplified products were sequenced on an ABI prism DNA sequencer using the BigDye terminator method. To find closely similar phylogenetic sequences, the generated sequence was sent into the BLAST algorithm of the National Center for Biological Information (NCBI) database. The program Mega 5.0's Neighbor-joining technique was used to build the phylogenetic tree.

### 2.3. Extracellular Biosynthesis of SeNPs

The fungal strain was maintained at  $28^\circ\text{C}$  on PDA slants (pH 6) with regular sub-culturing on new media. The stock culture, which was four days old, was inoculated into 250 mL Erlenmeyer flasks with 100 mL of MGYP medium (0.3% malt extract, 1.0% glucose, 0.3% yeast extract, and 0.5% peptone; pH 7.0). The inoculated flasks were then incubated on a rotary shaker for 4 days at  $28^\circ\text{C}$  (150 rpm). Centrifugation (5000 rpm, 15 min,  $4^\circ\text{C}$ ) was used to remove the fungus' mycelium from the culture medium, and the mycelium was then washed three times with sterile water. Typically, 10 g of fresh biomass was resuspended in 100 mL of sterile, deionized Milli-Q water and then incubated for a further 72 h while being stirred under the same circumstances as previously stated. Following

incubation, the cell-free filtrate was recovered after the biomass had been separated by filtering using Whatman filter paper no. 1. In order to create SeNPs, aqueous sodium selenite solution was added to reaction vessels containing cell-free filtrate at a final concentration of 1.0 mM. Then, without any light, the reaction vessels were incubated at 28 °C on a rotating shaker (150 rpm). Additionally, controls containing pure sodium selenite solution (without cell-free filtrate) as the negative control and controls containing cell-free filtrate (without sodium selenite) as the positive control were run concurrently with the experimental flask in 3 replications [54,55]. When SeNPs were successfully synthesized, the color of the mixture changed, and they were then collected by evaporating them in a rotary evaporator. The collected NPs residue was dried overnight at 200 °C in an oven.

#### 2.4. Characterization of SeNPs

The change in color in the Sodium selenite solution incubated with *A. terreus* was visually observed after UV-Visible spectroscopy analysis. The bioreduction of precursor Se ions was monitored by sampling aliquots (1 mL) at different time intervals. Absorption measurements were carried out on (JENWAY 6305 spectrophotometer) at a wavelength of 200–800 nm. For Fourier transform infrared (FTIR) spectroscopy investigations, the bio-transformed components discovered in the cell-free filtrate were dried and diluted with potassium bromide in a ratio of 1:100. The FTIR spectra of the samples were captured on an Agilent system (Cary 660 FTIR model). All measurements were carried out in the range of 400–4000  $\text{cm}^{-1}$ . The particle size, shape, and surface morphology were examined by transmission electron microscopy [41] and scanning electron microscopy [56], respectively. Transmission Electron Microscopy (TEM) images were obtained using (JEM-1230, Japan, Akishima, Tokyo 196-8558) at 120 kV. The colloidal solution of SeNPs was sprayed on a carbon-coated TEM copper grid and dried in the air before the examination. The surface morphology and elementary mapping of the synthesized Se-NPs were assessed by SEM-EDX analysis (JEOL, JSM-6360LA, Tokyo, Japan). The synthesized Se-NPs were loaded on holders followed by coating with gold by a sputter coater in a vacuum. The SEM was connected with an EDX instrument that was used for the qualitative and quantitative elemental composition of the sample. The texture of green fabricated SeNPs was recognized by field emission scanning electron microscopy (SEM, Quanta FEG250). The crystallinity of the biosynthesized SeNPs was tested by producing X-ray diffraction (XRD) patterns with an X-ray diffractometer, the X'Pert Pro (Philips, Eindhoven, Netherlands). The  $2\theta$  was within the range of 4°–80°. Ni-filtered Cu Ka radiation was used as the X-ray source. Voltage and current were 40 kV and 30 mA, respectively. The average size of the synthesized NPs was calculated using the Debye–Scherrer equation [57],

$$D = K\lambda/\beta\text{Cos}\theta \quad (1)$$

where, D is the mean particle size, K is the Scherrer's constant and equal to 0.9,  $\lambda$  is the X-ray wavelength,  $\beta$  is the half of the maximum intensity, and  $\theta$  is the Bragg's angle. The particle size distribution of SeNPs was evaluated using dynamic light scattering (DLS) measurements conducted with a Malvern Zetasizer Nanoseries compact scattering spectrometer (Malvern Instruments Ltd., Worcestershire, UK) and carried out at the Tabbin Institute for Metallurgical Studies, Cairo, Egypt. DLS analysis also provided more information about the homogeneity of the NPs solutions via the polydispersity index (PDI) measurement [58].

#### 2.5. Antimicrobial Activity

Antimicrobial activity of mycosynthesized SeNPs was evaluated against five microbial strains; *Escherichia coli* ATCC 25922, *Klebsiella Pneumonia* ATCC 13883, *Staphylococcus haemolyticus* ATCC 29970, *Staphylococcus aureus* ATCC 25923 and *Candida albicans* ATCC 90028 using the agar well diffusion method. Pure cultures of the tested bacteria were sub-cultured in nutrient broth and each strain was uniformly spread on sterilized petri plates with Muller-Hinton agar. Using a sterile cork borer, a circular well 7 mm in diameter was made in plates. To test the antibacterial activity, each well was loaded with (100  $\mu\text{L}$ ) of

SeNPs, and the plates were incubated at 37 °C overnight before the zones of inhibition were measured. Additionally, the antifungal activity of SeNPs was examined. The fungus strain was uniformly spread on potato dextrose agar (PDA) medium. Use a sterile cork-borer to make a 7 mm in diameter circular hole in the plate. To test antifungal activity, each well was filled with (100 µL) of Se-NPs, and the plate was incubated at 25 °C for 2–3 days before measuring the zone of inhibition [59].

### 2.6. Photocatalytic Degradation of Malachite Green Dye Using SeNPs

In a batch experiment using 100 mL of dye solution with a concentration of 100 ppm, the effectiveness of the biosynthesized SeNPs for malachite green dye treatment was evaluated. The batch experiment was performed in triplicate for each NPs concentration used (0.25, 0.50, 0.75 and 1.0 mg mL<sup>-1</sup>) in the presence of sunlight. All treatments were incubated at room temperature under aeration using a high-efficiency, low-pressure blower and a medium-bubble diffuser assembly. Color removal due to NPs treatment was measured at different time intervals (30.0, 60.0, 120.0, 180.0, 240.0 and 300.0 min) as follows: 1 mL of each treatment mixture was withdrawn and centrifuged at 5000 rpm for five minutes, and the optical density (O.D.) was measured at 624 nm using a spectrophotometer (721 spectrophotometer, M-ETCAL) [60]. The percentage (%) of color removal was measured using the following formula [61]:  $D(\%) = \frac{(\text{Dye}(i) - \text{Dye}(f))}{\text{Dye}(i)} \times 100$  (2) where D (%) is the decolorization percentage; Dye (i) is the initial absorbance; and Dye (f) is the final absorbance. Under ideal conditions, the reusability of the catalyst in malachite green dye degradation was achieved. For the fourth cycle. The catalyst was collected from the first cycle by centrifugation, washed twice with distilled water and oven-dried at 80 °C to remove water content before being used in the second cycle.

### 2.7. Statistical Analysis

Data were statistically analyzed using SPSS v18. A one-way analysis of variance (ANOVA) test was used for multiple sample comparisons, followed by a multiple comparison Tukey's Test for posthoc analysis for multiple comparison. Values were considered statistically significant at  $p < 0.05$ .

## 3. Results and Discussion

### 3.1. Isolation and Identification of the Fungal Isolate

The fungal isolate ASE1 was isolated from the soil, where it has the ability to synthesize SeNPs. According to the morphology and cultural characteristics, this fungal isolate was identified as *A. terreus*, where the diameter on PDA at 28 °C for 7 days was 35–40 mm, dark fleshy in surface color and yellow brown reverse color as illustrated in Figure 1 A,B. To confirm the morphological identification, the fungal isolate was identified genetically using the ITS region, where results confirmed the fungal isolate was identified as *A. terreus* with a similarity 99.5% (Figure 1C). Moreover, the sequence of *A. terreus* was recorded in the Gene bank with accession number OQ338186. Bafghi et al. [62] confirmed that, both *Aspergillus flavus* and *Candida albicans* have the ability to biosynthesize SeNPs using green and ecofriendly method. Moreover, Hashem et al. [54] reported that, *Penicillium expansum* has the ability to synthesize SeNPs.

### 3.2. Mycosynthesis of SeNPs

A green method for the synthesis of metal NPs has been employed as an alternative to the chemical and physical methods, as it is more cost effective, eco-friendly, easy to scale up, and does not need harsh conditions, such as hazardous chemicals and high temperatures [63]. In this study, *A. terreus* served as the bioreactor for the green synthesis of SeNPs. The free biomass filtrate solution color has changed after mixing with Na<sub>2</sub>SeO<sub>3</sub> from colorless to red, indicating the successful formation of SeNPs. The absence of the distinctive color shift in the negative control, pure sodium selenite solution devoid of cell-free filtrate, indicates that the synthesis is not a temperature- and time-dependent

process. Powdered SeNPs were obtained after calcination at 200 °C for 24 h. The bio-reduction of Se ions to form the nanoscale products may be attributed to the metabolites produced by *A. terreus* biomass filtrate [64]. Proteins and enzymes found in FBFs have been shown to play a critical role in the formation and stability of nanoparticles [58]. Islam, et al. [65] successfully biosynthesized SeNPs in Islam using *Fusarium oxysporum*, which were then tested for antifungal potency against the black mould *Aspergillus niger* and in-vivo biodistribution studies. By gamma-irradiating *Monascus purpureus*, SeNPs were biosynthesized and investigated for their biological assessment and photocatalytic capabilities [66].

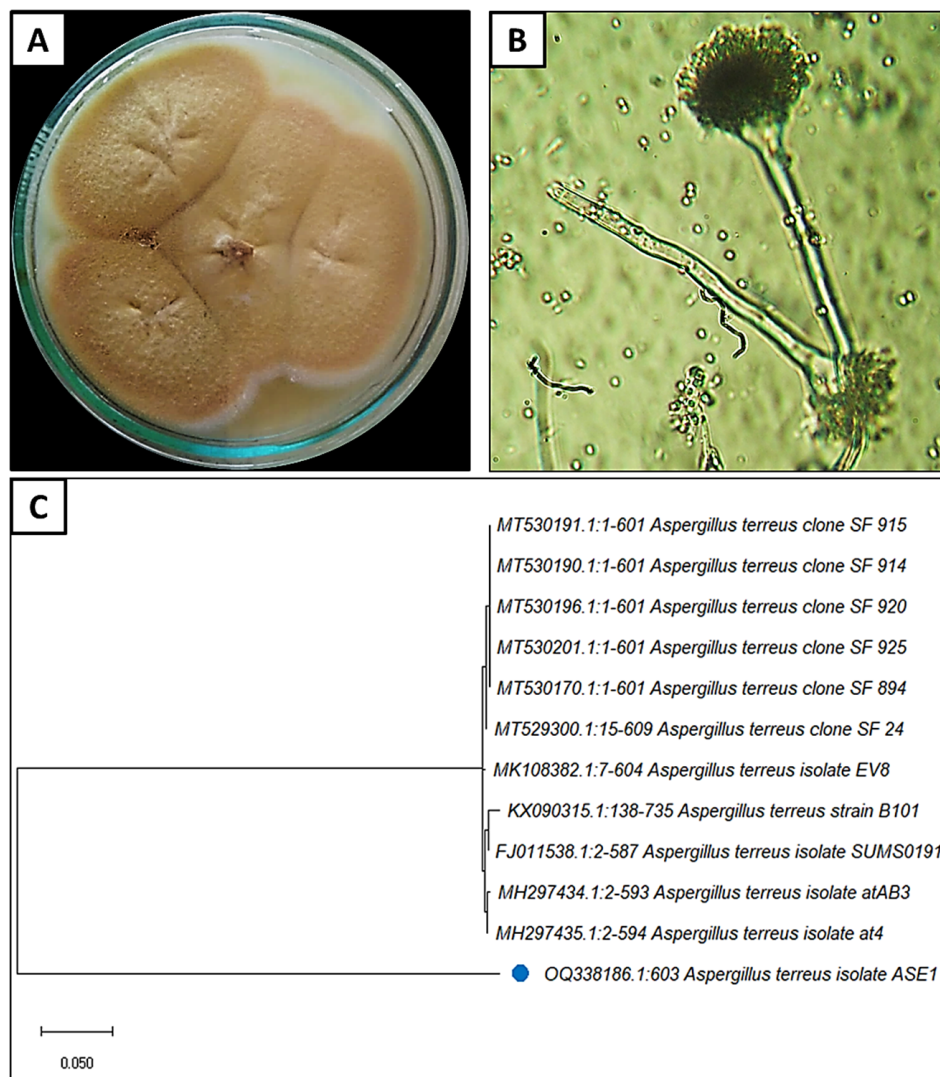


**Figure 1.** Identification of *A. terreus* (A–C): (A) fungus culture on PDA medium; (B) head, conidiophore, and conidia under bright field microscopy; (C) phylogenetic tree.

### 3.3. Characterization of SeNPs

#### 3.3.1. UV-Visible Spectroscopy

Utilizing UV-Visible spectroscopy, the colloidal solution of SeNPs was examined, and the development of a red color was seen between the wavelengths of 200 and 800 nm for *A. terreus* extract mediated SeNPs (Figure 2). Two absorption bands at 218 and 284 nm are observed and can be assigned to  $\text{Se}^0$ . The first absorption peak (at 218 nm) may be due to the inter band and core electronic transitions, or lower energy levels to conduction or higher bands. While the second peak (at 284 nm) is a consequence of coherent oscillation of free electrons from one surface of the Se particle to another known

as Surface Plasmon Resonance [67] absorption [68]. Generally, SeNPs possess size and shape-dependent properties. Previous studies have shown that SeNPs exhibit a variety of absorption bands in the UV-visible regime due to the applied synthetic protocols and the quantum confinement effect [69–71]. The data obtained show the efficacy of fungal extract used as a biocatalyst for the reduction of  $\text{SeO}_3^{2-}$  to  $\text{Se}^0$ . SeNPs were synthesized using *Acinetobacter* sp SW30 showed two absorption maxima at 300 nm and 500 nm [72]. Moreover, SeNPs revealed a significant absorption peak at 270 nm [73]. In the case of SeNPs produced by gamma-irradiated *Monascus purpureus*, the largest SPR peak was noted at 593 nm [66]. By employing *Fusarium oxysporum* as a biocatalyst, Islam et al. [65] demonstrated that the significant absorption peak at 265 nm suggested the synthesis of SeNPs. The spectra of green SeNPs showed absorbance at 265 nm by using an extract of the endophytic fungus, *Nigrospora gullinensis* [74]. The sharp peak of Se-NPs occurred at 295 nm fabricated by *Penicillium expansum* ATTC 36200 [54]. Kumar et al. [75] used a cell-free extract of *Geobacillus* to fabricate SeNPs and the SPR band was located at 349 nm. The inconsistency in these results might be due to a particle size variance. It is well established that the SPR bands are very susceptible and highly dependent on the nanoparticles size, shape,  $\text{Na}_2\text{SeO}_3$  concentration and the type of substrates presented in the biological extract [76].

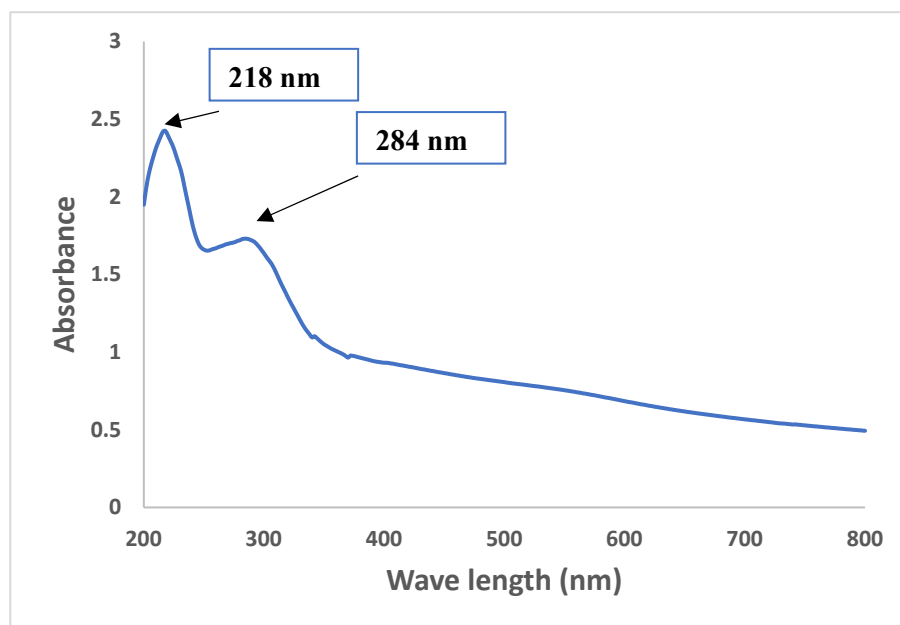


**Figure 2.** The UV-visible spectrum of biosynthesized SeNPs.

### 3.3.2. FT-IR Analysis

FTIR analysis was employed to examine the interaction between SeNPs and *A. terreus* supernatant, as illustrated in Figure 3. FT-IR spectra of the biosynthesized SeNPs showed intense absorption peaks at 3379.64, 1732.24, 1636.95, 1516.13, 1492.88, 1437.64, 1384.50, 1175.87, 1054.08, 894.33, 674.33, 604.08, 594.85, 509.41, 440.90, 421.83 and 410.27  $\text{cm}^{-1}$ . Peak at 3379.64  $\text{cm}^{-1}$  corresponded to the O–H stretching group of phenols and alcohol or N–H groups of amino acids in proteins [62,77,78]. The peak around 1732  $\text{cm}^{-1}$  corresponds to C=O stretching vibration, while the peaks observed at 1636.95, 1516.13, 1492.88, 1437.64  $\text{cm}^{-1}$  may be corresponded to the binding vibrations of the amide I band of proteins with N–H stretching, or may be attributed to the presence of aromatic substances such as polysaccharides [79,80]. The shifted one at 1384  $\text{cm}^{-1}$  is attributed to the C–H bending form in the alkanes. The peak observed at 1054.08  $\text{cm}^{-1}$  could represent C–O stretching of aliphatic ether [81]. The C=C functional group was also observed at 812  $\text{cm}^{-1}$ . Absorption peaks around 894.33, 674.33 and 604.08  $\text{cm}^{-1}$  may be due to the partial deuteration of amine or carboxyl group [82]. Finally, the calcinated SeNPs showed a peak at 509  $\text{cm}^{-1}$  [83]. These observations indicate the presence and binding of proteins with SeNPs which can lead to

their possible stabilization. It is important to understand though, that it is not just the size and shape of proteins, but the conformation of protein molecules that plays an important role [73]. Therefore, the proteins can interact with nanoparticles through their free amine groups or cysteine residues [84]. Furthermore, the proteins in the fungal extract might interact with the metal nanoparticles through their free amino or carboxyl groups [73].

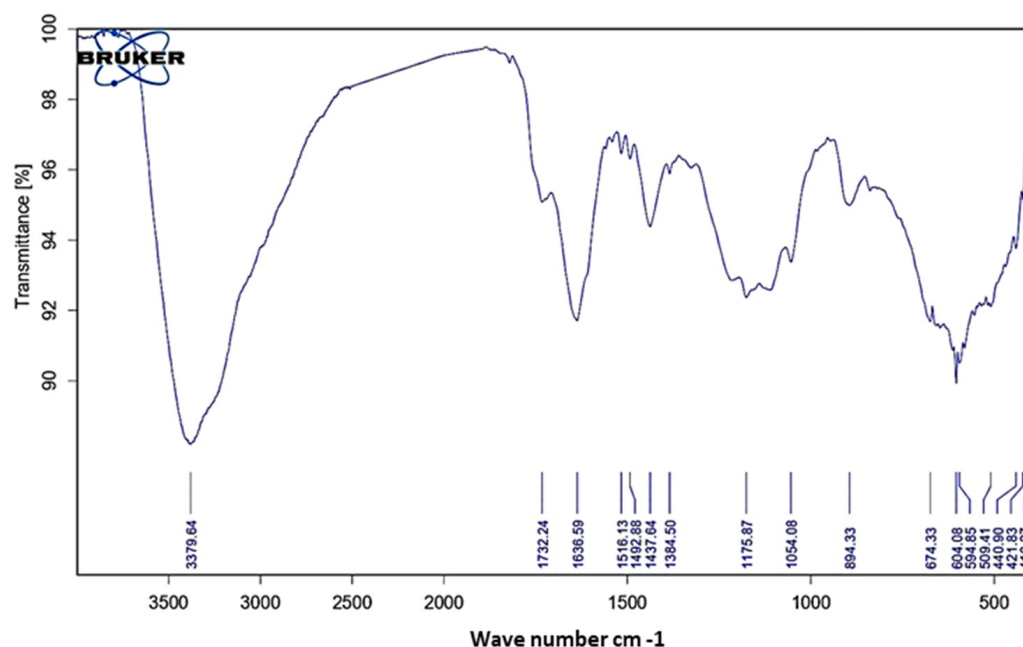


**Figure 3.** The FT-IR spectrum of mycosynthesized SeNPs fabricated by metabolites of *A. terreus*.

### 3.3.3. XRD Analysis

Figure 4A shows the XRD pattern of SeNPs synthesized by *A. terreus*. Five precise peaks were detected at  $2\theta$  degrees:  $23.92^\circ$  (100),  $30.8^\circ$  (101),  $41.84^\circ$  (111),  $51.44^\circ$  (201), and  $66.64^\circ$  (210) confirmed the crystalline phase of Se. Peaks observed at different  $2\theta$  values exhibited a monoclinic structure of SeNPs. The sharp peak at  $2\theta = 30.8^\circ$  (101), which showed significant orientation to the examined facet (101) and excellent purity of SeNPs after preparation, indicated that significant orientation had occurred. Debye-Scherrer equation was used to determine the average NPs size determined by XRD examination. The average SeNPs size obtained was 76.58 nm, and the FWHM ( $2\theta$ ) value was 0.11243. These agree with the results reported by Hashem et al. [54] which the average particle size ranged from 3 to 82 nm. Consistent with our findings, Al Jahdaly et al. [82] reported that the average size of SeNPs synthesized using green technology, as obtained by XRD analysis, was 37 nm. Hassanien et al. [81] calculated by XRD the average particle size of SeNPs synthesized by the *M. oleifera* aqueous extract was 18.85 nm.

### 3.3.4. DLS Analysis

DLS analysis is a critical technique for determining the size and size distribution of NPs in colloidal solutions. In this study, the average size of the biosynthesized SeNPs determined by DLS analysis was 50 nm (33% density) (Figure 4B). According to Bafghi et al. [62], the mean size of SeNPs demonstrated by PSA was between 51.5 and 64 nm. The polydispersity index (PDI) value was used to determine the homogeneity or heterogeneity of the NPs colloidal [58]. A PDI value less than 0.4 represents high homogeneity, while a higher value represents low homogeneity and a PDI value over 1 represent a heterogenous solution. In our study, a PDI value of 0.022 was obtained.

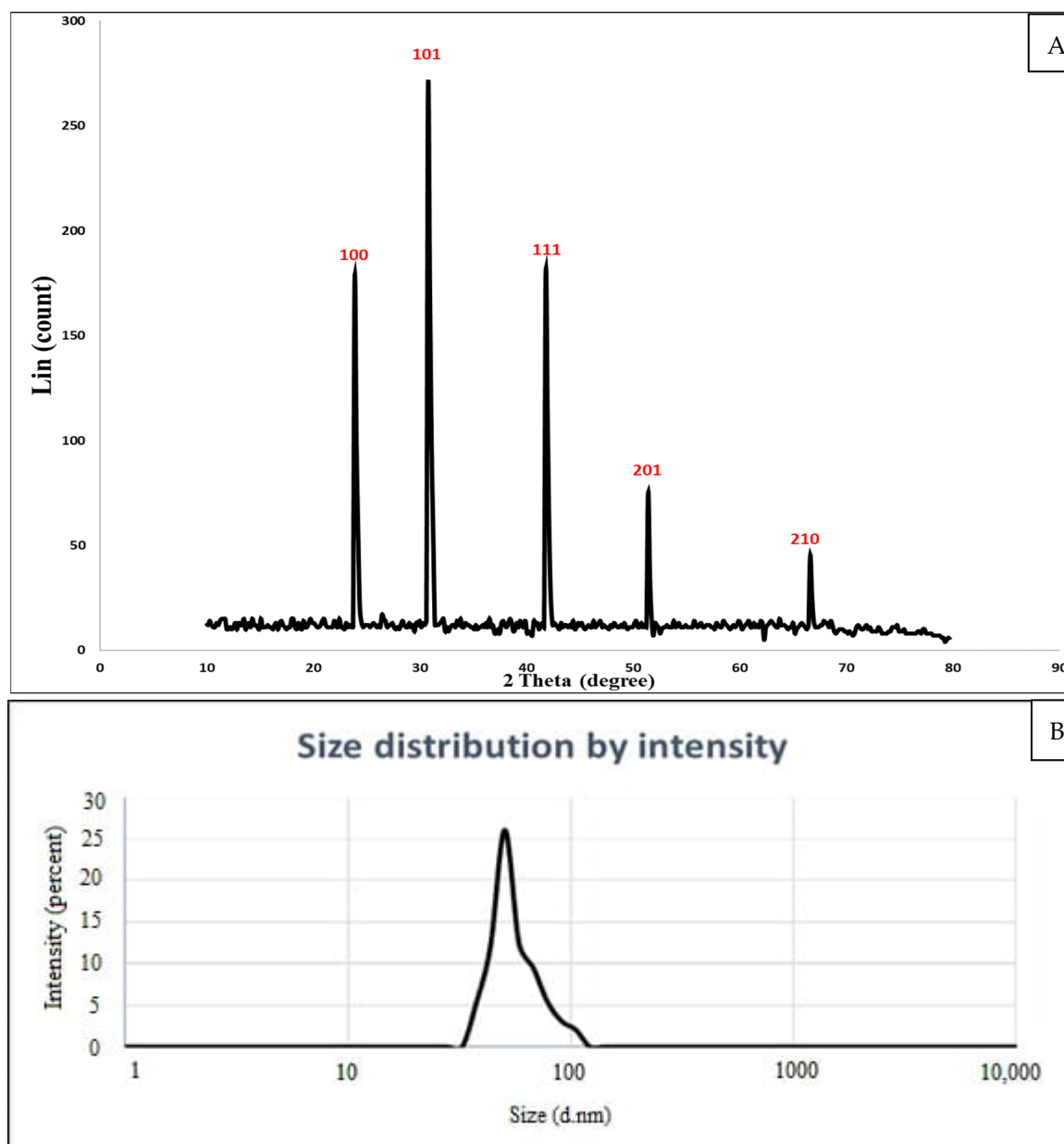


**Figure 4.** XRD analysis showed the crystalline nature (A); DLS analysis of mycosynthesized SeNPs (B).

### 3.3.5. TEM Analysis

TEM was used to examine the morphological characteristics of the NPs and their approximate size. The TEM analysis showed that the synthesized nanomaterial is spherical with a diameter of 10–100 nm (Figure 5). A study reported by Kumar et al. [75] showed that the synthesized nanomaterial is spherical with a diameter of 30–60 nm. Hassanien et al. [81] reported success in the formation of Se-NPLs from *M. oleifera* extract that were monodispersed in nature, spherical in shape, and ranged in size from 23 to 35. TEM analysis confirmed that biosynthesized SeNPs with unique structures could be produced using the substances present in FBF from *A. terreus* [65]. Further, the small size of the SeNPs synthesized in this work has the potential to be used in various biotechnological applications that depend on the NPs size.

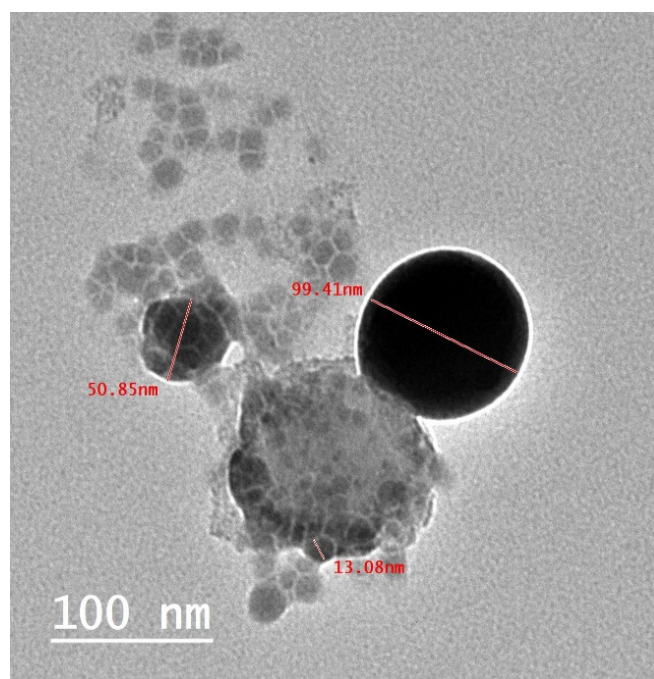


**Figure 5.** TEM image showed a spherical shape of biofabricated SeNPs by *A. terreus*.

### 3.3.6. Scanning Electron Microscopic-Energy-Dispersive X-ray (SEM-EDX)

Scanning electron microscopy was used to examine the morphological characteristics of green SeNPs. Accordingly, the green SeNPs had microspheres-shaped nanoparticles with a smooth surface, as displayed in Figure 6A,B which is the predominant shape of SeNPs agreed by reporting studies [73]. The scanning electron micrograph also revealed that the powder form particles are slightly agglomerated. A Few SeNPs were observed to be clustered to form larger particles. This result was in accordance with the SeNPs obtained in previous work [81]. The EDX profile of SeNPs confirmed the presence of Se element. According to the EDX profile (Figure 6C), the Se element is present at the weight percentages of 36.9%. The weight percentages of C, Cl, and Na are 18.9%, 6.5%, and 25.9%, respectively. The highest atomic percentages were for C (35.5%) followed by Se (33.8%).

### 3.4. Antimicrobial Activity

Antimicrobial impedance, which harms human health and increases the risk of diseases and the death rate associated with serious, life-threatening diseases, is currently the biggest health danger in every country in the world. Consequently, researchers studying the antibacterial effects of plants on bacteria that are resistant to several drugs are doing so in novel ways [85]. The use of SeNPs in the biomedical area has been increasing as an alternative to the growing bacterial resistance to antibiotics [76]. Inorganic Se has been shown to be highly harmful to humans when doses higher than the advised levels (0.07 mg/day for men and 0.06 mg/day for women) are consumed [86]. On the contrary, SeNPs represent a novel transport method and nanomedical application that minimizes potential harm to the organism [87]. Given that it has been demonstrated to possess antioxidant and antibacterial qualities, it could be utilized to treat a variety of ailments, including cancer, diabetes, and illnesses brought on by viruses and bacteria [88]. Because green nanoparticle synthesis is more affordable, environmentally benign, and produces a non-toxic substance that may be employed in a variety of medical applications, particularly in preventing the spread of antibiotic-resistant bacteria, it is preferred to chemical and physical processes. In the current study, mycosynthesized SeNPs were tested for antimicrobial activity against Gram-positive and negative bacteria, as well as unicellular fungi, using the agar well diffusion method, as shown in Figure 7. Our results revealed that, mycosynthesized SeNPs using *A. terreus* exhibited promising antibacterial activity against Gram-positive and Gram-negative

bacteria, where inhibition zones were 14, 20, 16 and 13 mm toward *S. haemolyticus* and *S. aureus*, *E. coli* and *K. pneumoniae* respectively as shown in Table 1. Also, mycosynthesized SeNPs had weak antifungal activity against *C. albicans* where inhibition zone was 12 mm (Table 1). On the other hand, CAZ, Flu and  $\text{Se}^+$  did not exhibit any activity on all tested bacterial and fungal strains. According to a previous study, *B. subtilis*, *S. pneumoniae*, *B. cereus*, *E. coli*, *P. mirabilis*, and *K. pneumoniae* could all be effectively stopped from growing when SeNPs was used. *B. subtilis* had the largest zone of inhibition (19 mm), followed by *E. coli* (15 mm), *B. cereus* (14 mm), *S. pneumoniae* (13 mm), and *P. mirabilis* (11 mm) [89]. In another study, the antifungal activity of SeNPs was assessed, and the inhibition zones for *A. niger* and *A. flavus* were 20 and 18 mm respectively, *C. albicans* did not show any discernible effects [90]. The creation of reactive oxygen species (ROS), breakdown of the bacterial cell wall, and suppression of protein and DNA synthesis are only a few of the potential modes of action for SeNPs [91].

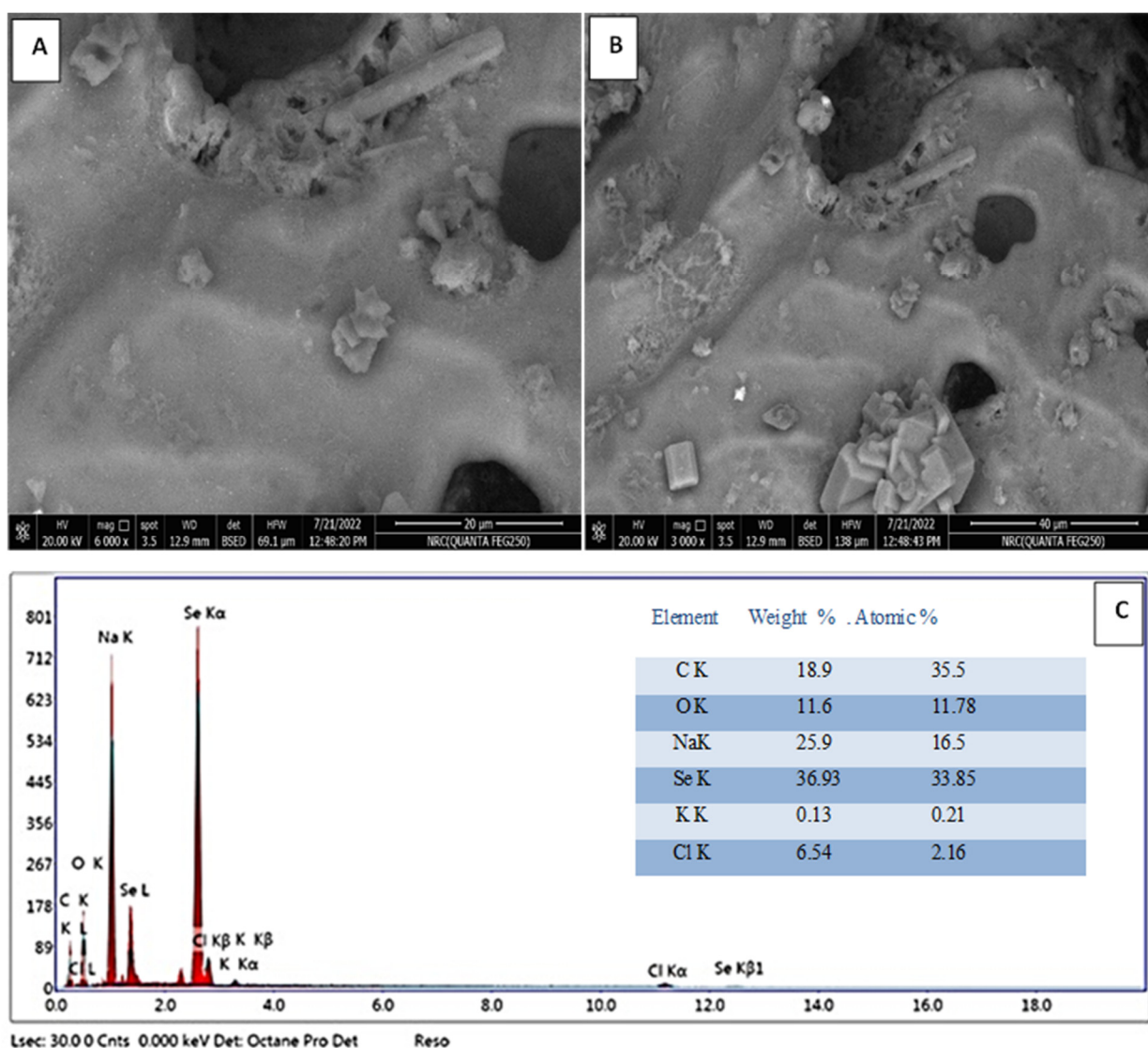


**Figure 6.** (A,B) SEM images of SeNPs in which the nanoparticle was spherical in shape confirmed that SeNPs are in the nano-regime. (C) EDX spectrum showed elemental compositions of as-formed SeNPs.

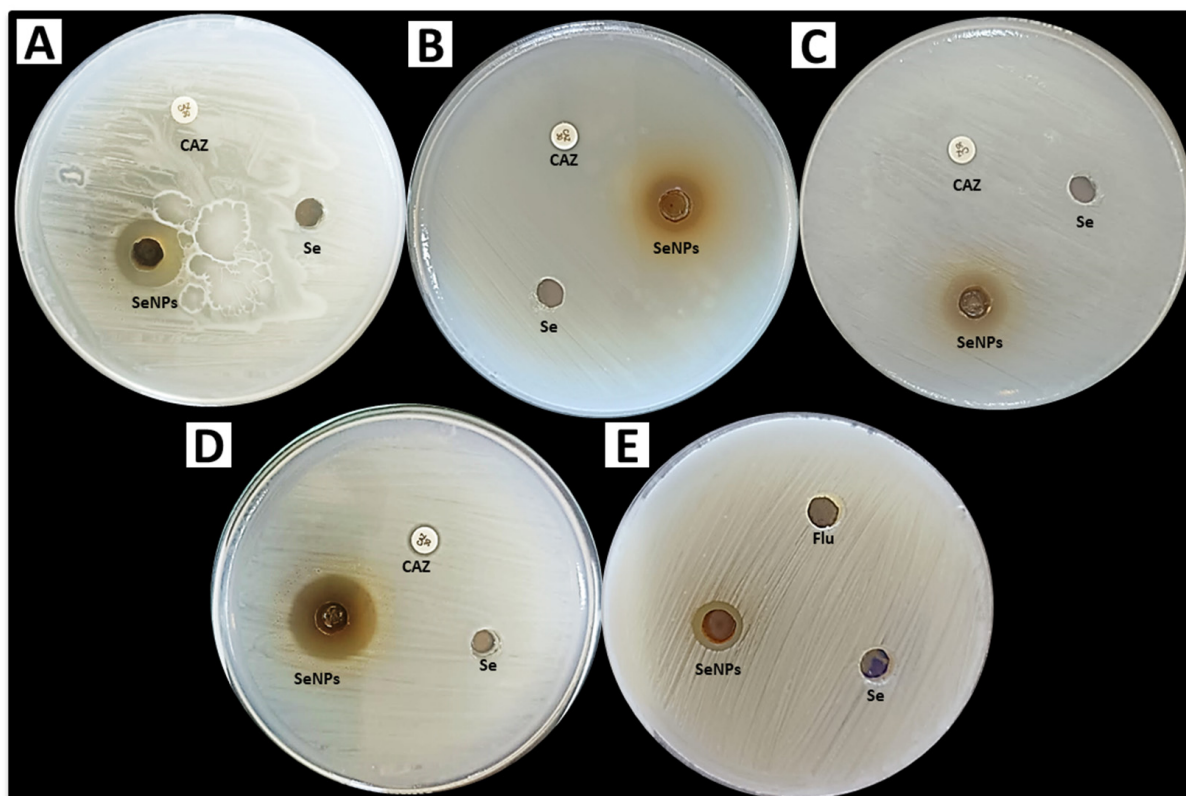


**Figure 7.** Antimicrobial activity of mycosynthesized SeNPs and sodium selenite (Se) against *E. coli* (A), *K. pneumonia* (B), *S. haemolyticus* (C), *S. aureus* (D), and *C. albicans* (E).

**Table 1.** Inhibition zones of mycosynthesized SeNPs against all tested microbial strains.

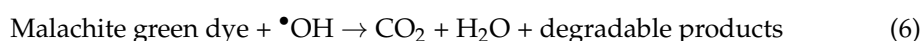
Microbial Strain	Inhibition Zone/mm		
	Se (1000 µg/mL)	SeNPs (1000 µg/mL)	CAZ/FLU
<i>E. coli</i>	ND	16	ND
<i>K. pneumonia</i>	ND	13	ND
<i>S. haemolyticus</i>	ND	14	ND
<i>S. aureus</i>	ND	20	8
<i>C. albicans</i>	ND	12	ND

### 3.5. Photocatalytic Activity

The potency of the biosynthesized SeNPs for decolorization and degradation of malachite green dye was investigated at different incubation times (0.0, 60.0, 120.0, 180.0, 240.0 and 300.0 min.), and at different NPs concentrations (0.25, 0.50, 0.75 and 1.0 mg mL<sup>-1</sup> malachite green dye) in sunlight. Data shown in Figure 8 indicated that the function of SeNPs as a biocatalyst for dye degradation was dose- and time-dependent. At a concentration of 0.25 mg SeNPs, the decolorization percentages were 29.3 ± 0.03, 42.5 ± 0.02, and 43.2 ± 0.01% after 60.0, 180.0, and 240.0 min, respectively. Increasing the SeNPs concentration to 0.50, 0.75, and 1.0 mg, has increased the decolorization percentages to 66.6 ± 0.02, 80.3 ± 0.02, and 89.1 ± 0.03%, respectively, after 240 min, as compared with the control for the same time (7.6 ± 0.01%). However, these results were not significant as compared with the decolorization percentages for the same concentrations after 300.0 min. Therefore, 1.0 mg mL<sup>-1</sup> SeNPs achieved the high decolorization percentage of malachite green dye after 240.0 min. These results are due to the existence of more adsorption sites on the NPs surface [92]. Decolorization strategies and time required for decolorization were found to

be related to various parameters such as dye type, sorbent type, and concentration [93]. Similarly, the photocatalytic activity of SeNPs was studied by El-Sayed et al. [66]. According to Cittrarasu, et al. [94] the decolorization efficiency of MB was steadily increased with higher irradiation times (up to 80 min). Fouda et al. [58] reported that the efficacy of biosynthesized MgONPs in degrading textile wastewater should be achieved in the presence of light as stimulators. Akinola et al. [95] success in the degrading of malachite green dye by 88.25–93.24% by using Ti-AgNPs mediated by aqueous leaf, pod, seed and seed shell extracts of *Cola nitida*. El-Naggar and Shoueir [96] reported that the metal oxides of NPs have the efficacy to induce charge separation by absorbing the light, hence forming holes that reduce or oxidize the organic substances including organic dyes. The photocatalytic activities in this study are caused by the activation of biosynthesized SeNPs by sunlight stimulators, which is followed by the production of photoexcited electrons that are transferred from the valence band to the conduction band, resulting in the formation of  $\bullet\text{O}^{2-}$  radicals. Furthermore, the forming holes react with  $\text{H}_2\text{O}$  and form hydrogen ( $\text{H}^+$ ) ions and hydroxyl radicals ( $\bullet\text{OH}$ ), which are considered highly active oxidizing agents used in the degradation of dyes [97].

The mechanism for the degradation of malachite green dye begins with the adsorption of malachite green dye ions by SeNPs, followed by the activation of the degradation by a UV-lamp, which stimulates photo-regenerated electrons in the C.B area. Consequently, the photo-regenerated electrons in the V.B were easily migrating to the surface of SeNPs to trigger redox reactions [82]. The holes reacted with water or  $\text{HO}^-$ , which rapidly adsorbed onto the SeNPs surface to form  $\text{OH}^*$  radicals. The superoxide oxyanion radicals  $\text{O}_2^{-*}$  being observed by the reacting of electrons  $e^-$  with  $\text{O}_2$ , and  $\text{O}_2^{-*}$  reacted with  $\text{h}^+$  to promote peroxide radicals of  $\text{HOO}^*$ . All these powerfully active species  $\text{OH}^*$ ,  $\text{O}_2^{-*}$ , and  $\text{h}^+$  deplete malachite green dye molecules into  $\text{H}_2\text{O}$ ,  $\text{CO}_2$ , and minerals (colorless products) through a series of redox reactions [98,99].



### 3.6. Recyclability Test

The photocatalyst stability or reusability is the critical factor for integration into industrial applications. In the current study, the reusability of green synthesized SeNPs in the photodegradation of malachite green dye was achieved under optimum conditions (in the presence of light irradiation at a concentration of 100 ppm of dye, 1.0 mg mL<sup>-1</sup> SeNPs for 240.0 min). The reusability test was measured for the fourth cycle. Data analysis revealed that the activity of the catalyst was decreased and measured after four cycles. The photodegradation of malachite green dye was 89% after the first cycle and decreased to 71% after the fourth cycle (Figure 9). These reductions in photocatalyst activity can be related to the saturated sites that exist on the surface of catalysts with small intermediate biodegradable compounds [100]. Fouda et al. [58] reported that the photodegradation was reduced from 89% after the first cycle to 86% after the fourth cycle of crude textile wastewater. Based on the obtained data, it can be concluded that the high stability of green synthesized SeNPs enhanced the photodegradation of malachite green dye for different cycles.

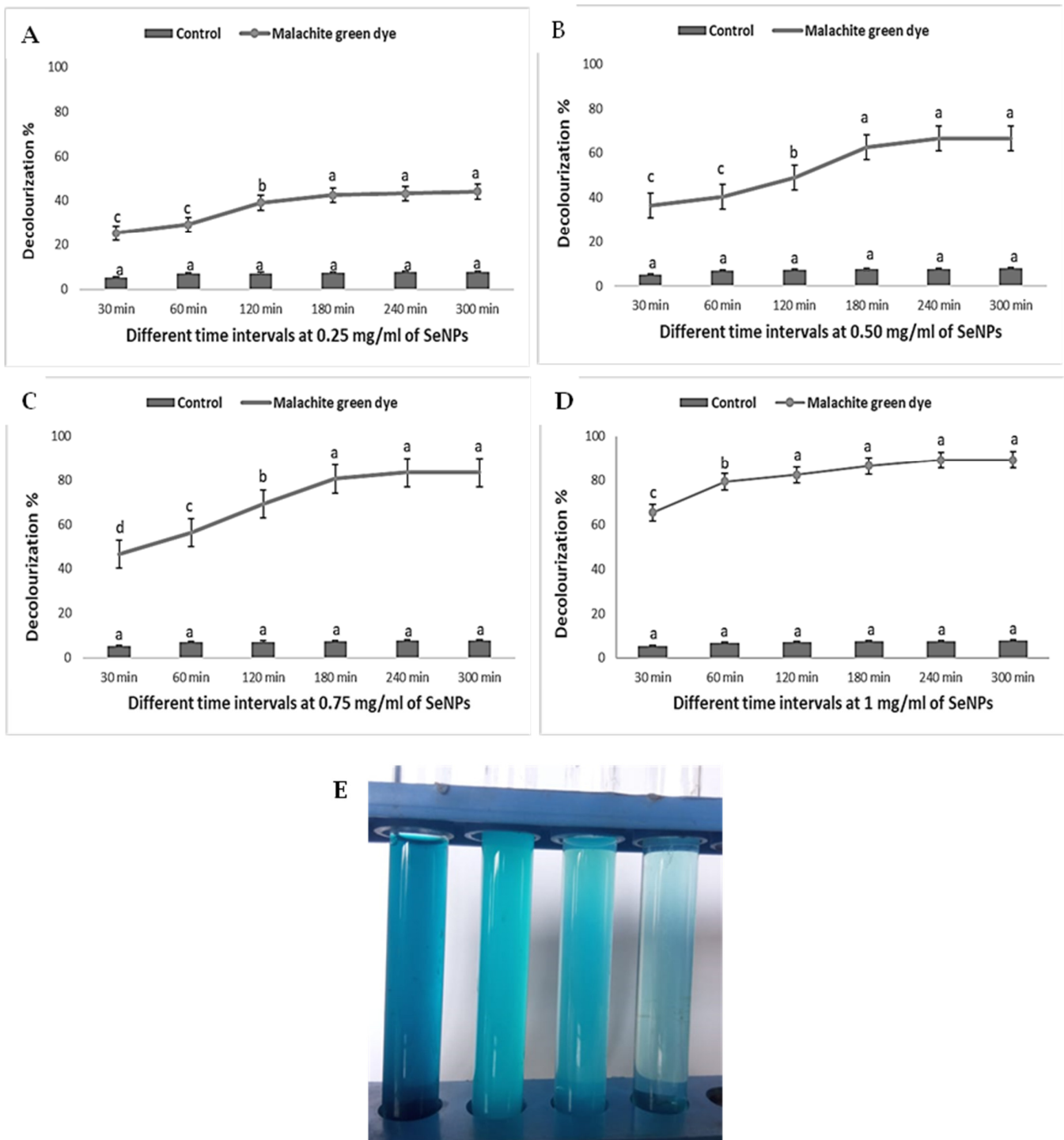


**Figure 8.** Decolorization percentages (%) of malachite green dye at different concentrations of SeNPs 0.24 (A), 0.5 (B), 0.75 (C), and 1 mg/mL (D); and the change of color removal of MG dye at different times (E). Letters a, b, c, d Mean significance power.

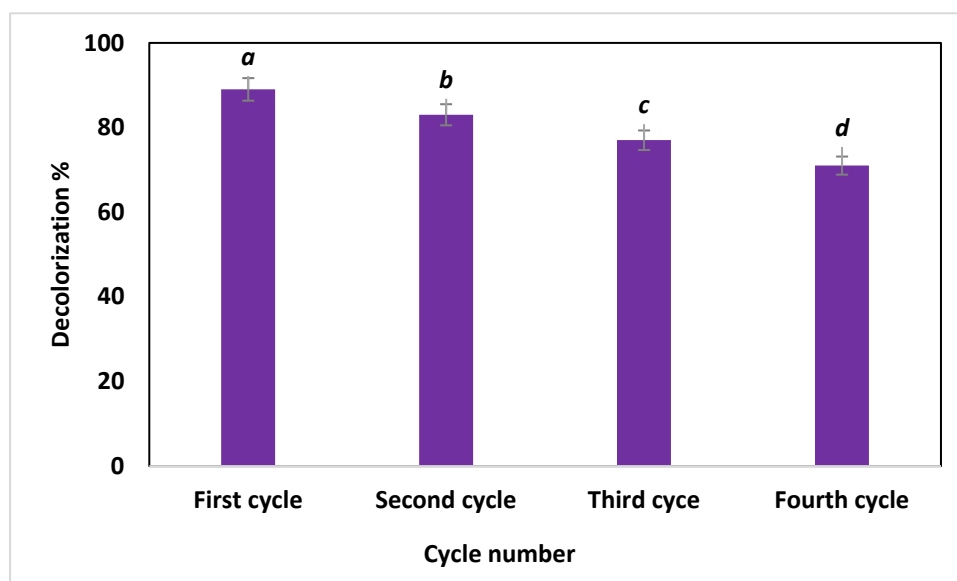


**Figure 9.** The reusability assessment of SeNPs for decolorization of malachite green dye After 240.0 min. Letters a, b, c, d Mean significance power.

#### 4. Conclusions

In this study, SeNPs were successfully synthesized using a cell-free extract of *A. terreus* using an eco-friendly method. The prepared SeNPs were fully characterized using Uv-Vis, FTIR, XRD, DLS, TEM, and SEM analyses. The characterization results revealed that SeNPs in nano form have a spherical shape with a size of less than 100 nm. Moreover, antimicrobial and photocatalytic activities were assessed. Results illustrated that SeNPs have antimicrobial activity against Gram-positive and Gram-negative bacteria as well as unicellular fungi, where inhibition zones were in the range of 12–20 mm. Furthermore, SeNPs had promising photocatalytic activity, with up to 89% biodegradation of malachite green dye after 240 min. Herein, the mycosynthesized SeNPs using a cell-free extract of *A. terreus* had antimicrobial as well as photocatalytic activities, which can be used in medical and environmental applications.

**Author Contributions:** E.S.: Conceptualization, Methodology, Formal analysis, and investigation, Writing—original draft preparation, Writing—review and editing, Resources, Software; A.E.M.: Methodology, Writing—original draft preparation; A.A.A.-A.: Funding, Writing—review and editing; A.F.H.: Methodology; A.A.E.-b.: Methodology; M.A.: Methodology; A.W.: Methodology; T.N.: Methodology; M.M.F.: Writing—review and editing; A.A.A.: Resources, Software, Writing—review and editing; A.H.H.: Conceptualization, Methodology, Formal analysis, and investigation, Writing—original draft preparation, Writing—review and editing, Resources, Software. All authors have read and agreed to the published version of the manuscript.

**Funding:** The authors extend their appreciation to the researcher supporting project number (RSP2023R505), King Saud University, Riyadh, Saudi Arabia.

**Data Availability Statement:** The datasets generated during and/or analyzed during the current study are available from the corresponding author upon reasonable request.

**Acknowledgments:** The authors express their sincere thanks to the Faculty of Science (Boys), Al-Azhar University, Cairo, Egypt, for providing the necessary research facilities. The authors extend their appreciation to the researcher supporting project number (RSP2023R505), King Saud University, Riyadh, Saudi Arabia, for funding this work.

**Conflicts of Interest:** The authors declare no conflict of interest.

## References

1. Sathya, R.; Arasu, M.V.; Al-Dhabi, N.A.; Vijayaraghavan, P.; Ilavenil, S.; Rejiniemon, T. Towards sustainable wastewater treatment by biological methods—A challenges and advantages of recent technologies. *Urban Clim.* **2023**, *47*, 101378. [[CrossRef](#)]
2. Nachana'a Timothy, E.T.W. Environmental pollution by heavy metal: An overview. *Chemistry* **2019**, *3*, 72–82.
3. Tianzhi, W.; Weijie, W.; Hongying, H.; Khu, S.-T. Effect of coagulation on bio-treatment of textile wastewater: Quantitative evaluation and application. *J. Clean. Prod.* **2021**, *312*, 127798. [[CrossRef](#)]
4. Liu, L.; Chen, Z.; Zhang, J.; Shan, D.; Wu, Y.; Bai, L.; Wang, B. Treatment of industrial dye wastewater and pharmaceutical residue wastewater by advanced oxidation processes and its combination with nanocatalysts: A review. *J. Water Process. Eng.* **2021**, *42*, 102122. [[CrossRef](#)]
5. Mehta, M.; Sharma, M.; Pathania, K.; Jena, P.K.; Bhushan, I. Degradation of synthetic dyes using nanoparticles: A mini-review. *Environ. Sci. Pollut. Res.* **2021**, *28*, 49434–49446. [[CrossRef](#)]
6. Pavithra, K.G.; Jaikumar, V.J.; Chemistry, E. Removal of colorants from wastewater: A review on sources and treatment strategies. *J. Ind. Eng. Chem.* **2019**, *75*, 1–19. [[CrossRef](#)]
7. Ismail, M.; Akhtar, K.; Khan, M.I.; Kamal, T.; Khan, M.A.; Asiri, A.M.; Seo, J.; Khan, S.B. Pollution, Toxicity and Carcinogenicity of Organic Dyes and their Catalytic Bio-Remediation. *Curr. Pharm. Des.* **2019**, *25*, 3645–3663. [[CrossRef](#)]
8. Shindhal, T.; Rakholiya, P.; Varjani, S.; Pandey, A.; Ngo, H.H.; Guo, W.; Ng, H.Y.; Taherzadeh, M.J. A critical review on advances in the practices and perspectives for the treatment of dye industry wastewater. *Bioengineered* **2020**, *12*, 70–87. [[CrossRef](#)]
9. Yadav, S.; Yadav, A.; Bagothia, N.; Sharma, A.K.; Kumar, S. Adsorptive potential of modified plant-based adsorbents for sequestration of dyes and heavy metals from wastewater—A review. *J. Water Process. Eng.* **2021**, *42*, 102148. [[CrossRef](#)]
10. Dutta, S.; Gupta, B.; Srivastava, S.K.; Gupta, A.K. Recent advances on the removal of dyes from wastewater using various adsorbents: A critical review. *Mater. Adv.* **2021**, *2*, 4497–4531. [[CrossRef](#)]
11. Hamad, H.N.; Idrus, S. Recent Developments in the Application of Bio-Waste-Derived Adsorbents for the Removal of Methylene Blue from Wastewater: A Review. *Polymers* **2022**, *14*, 783. [[CrossRef](#)]
12. Saravanan, A.; Kumar, P.S.; Karishma, S.; Vo, D.-V.N.; Jeevanantham, S.; Yaashikaa, P.; George, C.S. A review on biosynthesis of metal nanoparticles and its environmental applications. *Chemosphere* **2020**, *264*, 128580. [[CrossRef](#)] [[PubMed](#)]
13. Hashem, A.H.; Saied, E.; Hasanin, M.S. Green and ecofriendly bio-removal of methylene blue dye from aqueous solution using biologically activated banana peel waste. *Sustain. Chem. Pharm.* **2020**, *18*, 100333. [[CrossRef](#)]
14. Saravanan, A.; Kumar, P.S.; Hemavathy, R.; Jeevanantham, S.; Jawahar, M.J.; Neshaanthini, J. A review on synthesis methods and recent applications of nanomaterial in wastewater treatment: Challenges and future perspectives. *Chemosphere* **2022**, *307*, 135713. [[CrossRef](#)] [[PubMed](#)]
15. Dong, X.; Li, Y.; Li, D.; Liao, D.; Qin, T.; Prakash, O.; Kumar, A.; Liu, J.-Q. A new 3D 8-connected Cd(ii) MOF as a potent photocatalyst for oxytetracycline antibiotic degradation. *Crystengcomm* **2022**, *24*, 6933–6943. [[CrossRef](#)]
16. Zheng, M.; Chen, J.; Zhang, L.; Cheng, Y.; Lu, C.; Liu, Y.; Singh, A.; Trivedi, M.; Kumar, A.; Liu, J. Metal organic frameworks as efficient adsorbents for drugs from wastewater. *Mater. Today Commun.* **2022**, *31*, 103514. [[CrossRef](#)]
17. Ahmed, S.; Mofijur, M.; Nuzhat, S.; Chowdhury, A.T.; Rafa, N.; Uddin, A.; Inayat, A.; Mahlia, T.; Ong, H.C.; Chia, W.Y.; et al. Recent developments in physical, biological, chemical, and hybrid treatment techniques for removing emerging contaminants from wastewater. *J. Hazard. Mater.* **2021**, *416*, 125912. [[CrossRef](#)] [[PubMed](#)]
18. Aswathi, V.P.; Meera, S.; Maria, C.G.A.; Nidhin, M. Green synthesis of nanoparticles from biodegradable waste extracts and their applications: A critical review. *Nanotechnol. Environ. Eng.* **2022**, 1–21. [[CrossRef](#)]
19. Ifijen, I.H.; Maliki, M.; Anegebe, B. Synthesis, photocatalytic degradation and antibacterial properties of selenium or silver doped zinc oxide nanoparticles: A detailed review. *Opennano* **2022**, *8*, 100082. [[CrossRef](#)]
20. Somu, P.; Paul, S. Protein assisted one pot controlled synthesis of monodispersed and multifunctional colloidal silver-gold alloy nanoparticles. *J. Mol. Liq.* **2019**, *291*, 111303. [[CrossRef](#)]
21. Hasanin, M.; Hashem, A.H.; Lashin, I.; Hassan, S.A.M. In vitro improvement and rooting of banana plantlets using antifungal nanocomposite based on myco-synthesized copper oxide nanoparticles and starch. *Biomass Convers. Biorefinery* **2021**, 1–11. [[CrossRef](#)]
22. Shehabeldine, A.M.; Hashem, A.H.; Wassel, A.R.; Hasanin, M. Antimicrobial and Antiviral Activities of Durable Cotton Fabrics Treated with Nanocomposite Based on Zinc Oxide Nanoparticles, Acyclovir, Nanochitosan, and Clove Oil. *Appl. Biochem. Biotechnol.* **2021**, *194*, 783–800. [[CrossRef](#)]
23. Al-Gheethi, A.A.S.; Mohamed, R.M.S.R.; Noman, E.A.; Kassim, A.H.M. *Prospects of Fresh Market Wastes Management in Developing Countries*; Springer: Berlin/Heidelberg, Germany, 2020.
24. Lashin, I.; Hasanin, M.; Hassan, S.A.M.; Hashem, A.H. Green biosynthesis of zinc and selenium oxide nanoparticles using callus extract of *Ziziphus spina-christi*: Characterization, antimicrobial, and antioxidant activity. *Biomass Convers. Biorefinery* **2021**, 1–14. [[CrossRef](#)]
25. Abdelaziz, A.M.; Salem, S.S.; Khalil, A.M.A.; El-Wakil, D.A.; Fouda, H.M.; Hashem, A.H. Potential of biosynthesized zinc oxide nanoparticles to control Fusarium wilt disease in eggplant (*Solanum melongena*) and promote plant growth. *Biometals* **2022**, *35*, 601–616. [[CrossRef](#)]

26. El-Naggar, M.E.; Hasanin, M.; Hashem, A.H. Eco-Friendly Synthesis of Superhydrophobic Antimicrobial Film Based on Cellulose Acetate/Polycaprolactone Loaded with the Green Biosynthesized Copper Nanoparticles for Food Packaging Application. *J. Polym. Environ.* **2021**, *30*, 1820–1832. [[CrossRef](#)]
27. Hashem, A.H.; Al Abboud, M.A.; Alawlaqi, M.M.; Abdelghany, T.M.; Hasanin, M. Synthesis of Nanocapsules Based on Biosynthesized Nickel Nanoparticles and Potato Starch: Antimicrobial, Antioxidant, and Anticancer Activity. *Starch-Stärke* **2021**, *74*, 2100165. [[CrossRef](#)]
28. Hashem, A.H.; Selim, T.A.; Alruhaili, M.H.; Selim, S.; Alkhalifah, D.H.M.; Al Jaouni, S.K.; Salem, S.S. Unveiling Antimicrobial and Insecticidal Activities of Biosynthesized Selenium Nanoparticles Using Prickly Pear Peel Waste. *J. Funct. Biomater.* **2022**, *13*, 112. [[CrossRef](#)] [[PubMed](#)]
29. Ali, O.M.; Hasanin, M.S.; Suleiman, W.B.; Helal, E.E.-H.; Hashem, A.H. Green biosynthesis of titanium dioxide quantum dots using watermelon peel waste: Antimicrobial, antioxidant, and anticancer activities. *Biomass Convers. Biorefinery* **2022**, 1–12. [[CrossRef](#)]
30. Rahuman, H.B.H.; Dhandapani, R.; Narayanan, S.; Palanivel, V.; Paramasivam, R.; Subbarayalu, R.; Thangavelu, S.; Muthupandian, S. Medicinal plants mediated the green synthesis of silver nanoparticles and their biomedical applications. *IET Nanobiotechnol.* **2022**, *16*, 115–144. [[CrossRef](#)]
31. Jayarambabu, N.; Rao, T.V.; Kumar, R.R.; Akshaykranth, A.; Shanker, K.; Suresh, V. Anti-hyperglycemic, pathogenic and anticancer activities of Bambusa arundinacea mediated Zinc Oxide nanoparticles. *Mater. Today Commun.* **2020**, *26*, 101688. [[CrossRef](#)]
32. Simon, S.; Sibuyi, N.R.S.; Fadaka, A.O.; Meyer, S.; Josephs, J.; Onani, M.O.; Meyer, M.; Madiehe, A.M. Biomedical Applications of Plant Extract-Synthesized Silver Nanoparticles. *Biomedicines* **2022**, *10*, 2792. [[CrossRef](#)] [[PubMed](#)]
33. Hashem, A.H.; Saied, E.; Amin, B.H.; Alotibi, F.O.; Al-Askar, A.A.; Arishi, A.A.; Elkady, F.M.; Elbahnasawy, M.A. Antifungal Activity of Biosynthesized Silver Nanoparticles (AgNPs) against *Aspergilli* Causing Aspergillosis: Ultrastructure Study. *J. Funct. Biomater.* **2022**, *13*, 242. [[CrossRef](#)] [[PubMed](#)]
34. Hashem, A.H.; Saied, E.; Ali, O.M.; Selim, S.; Al Jaouni, S.K.; Elkady, F.M.; El-Sayyad, G.S. Pomegranate Peel Extract Stabilized Selenium Nanoparticles Synthesis: Promising Antimicrobial Potential, Antioxidant Activity, Biocompatibility, and Hemocompatibility. *Appl. Biochem. Biotechnol.* **2023**, 1–24. [[CrossRef](#)] [[PubMed](#)]
35. Abu-Elghait, M.; Hasanin, M.; Hashem, A.H.; Salem, S.S. Ecofriendly novel synthesis of tertiary composite based on cellulose and myco-synthesized selenium nanoparticles: Characterization, antibiofilm and biocompatibility. *Int. J. Biol. Macromol.* **2021**, *175*, 294–303. [[CrossRef](#)]
36. Hasanin, M.S.; Hashem, A.H.; El-Sayed, E.S.A.; El-Saied, H. Green ecofriendly bio-deinking of mixed office waste paper using various enzymes from *Rhizopus microsporus* AH3: Efficiency and characteristics. *Cellulose* **2020**, *27*, 4443–4453. [[CrossRef](#)]
37. Hashem, A.H.; Suleiman, W.B.; Abu-Elreesh, G.; Shehabeldine, A.M.; Khalil, A.M.A. Sustainable lipid production from oleaginous fungus *Syncephalastrum racemosum* using synthetic and watermelon peel waste media. *Bioresour. Technol. Rep.* **2020**, *12*, 100569. [[CrossRef](#)]
38. Hashem, A.H.; Abu-Elreesh, G.; El-Sheikh, H.H.; Suleiman, W.B. Isolation, identification, and statistical optimization of a psychrotolerant *Mucor racemosus* for sustainable lipid production. *Biomass Convers. Biorefinery* **2022**, *13*, 3415–3426. [[CrossRef](#)]
39. Hashem, A.H.; Khattab, A.M.; Abdelraof, M. A facile one-pot bioconversion of frying oil waste to single cell oils and related products using fungi via response surface methodology. *Biomass Convers. Biorefinery* **2022**, 1–11. [[CrossRef](#)]
40. Peramune, D.; Manatunga, D.C.; Dassanayake, R.S.; Premalal, V.; Liyanage, R.N.; Gunathilake, C.; Abidi, N. Recent advances in biopolymer-based advanced oxidation processes for dye removal applications: A review. *Environ. Res.* **2022**, *215*, 114242. [[CrossRef](#)]
41. Jeon, J.; Kweon, D.H.; Jang, B.J.; Ju, M.J.; Baek, J. Enhancing the Photocatalytic Activity of TiO<sub>2</sub> Catalysts. *Adv. Sustain. Syst.* **2020**, *4*, 202000197. [[CrossRef](#)]
42. Sobhani, A.; Salavati-Niasari, M. Transition metal selenides and diselenides: Hydrothermal fabrication, investigation of morphology, particle size and their applications in photocatalyst. *Adv. Colloid Interface Sci.* **2021**, *287*, 102321. [[CrossRef](#)] [[PubMed](#)]
43. Morán-Serradilla, C.; Angulo-Elizari, E.; Henriquez-Figueroa, A.; Sanmartín, C.; Sharma, A.K.; Plano, D.J.M. Seleno-metabolites and their precursors: A new dawn for several illnesses? *Metabolites* **2022**, *12*, 874. [[CrossRef](#)] [[PubMed](#)]
44. Hariharan, S.; Dharmaraj, S. Selenium and selenoproteins: It's role in regulation of inflammation. *Inflammopharmacology* **2020**, *28*, 667–695. [[CrossRef](#)]
45. Bhattacharya, S. Protective Role of the Essential Trace Elements in the Obviation of Cadmium Toxicity: Glimpses of Mechanisms. *Biol. Trace Element Res.* **2021**, *200*, 2239–2246. [[CrossRef](#)]
46. Bisht, N.; Phalswal, P.; Khanna, P.K. Selenium nanoparticles: A review on synthesis and biomedical applications. *Mater. Adv.* **2021**, *3*, 1415–1431. [[CrossRef](#)]
47. Sarkar, J.; Mridha, D.; Davoodbasha, M.A.; Banerjee, J.; Chanda, S.; Ray, K.; Roychowdhury, T.; Acharya, K.; Sarkar, J. A State-of-the-Art Systemic Review on Selenium Nanoparticles: Mechanisms and Factors Influencing Biogenesis and Its Potential Applications. *Biol. Trace Element Res.* **2023**, 1–37. [[CrossRef](#)]
48. Stater, E.P.; Sonay, A.Y.; Hart, C.; Grimm, J. The ancillary effects of nanoparticles and their implications for nanomedicine. *Nat. Nanotechnol.* **2021**, *16*, 1180–1194. [[CrossRef](#)] [[PubMed](#)]

49. Truong, L.; Medina-Cruz, D.; Mostafavi, E.; Rabiee, N. Selenium Nanomaterials to Combat Antimicrobial Resistance. *Molecules* **2021**, *26*, 3611. [[CrossRef](#)] [[PubMed](#)]
50. Makhlof, M.E.M.; Albalwe, F.M.; Al-Shaikh, T.M.; El-Sheekh, M.M. Suppression Effect of *Ulva lactuca* Selenium Nanoparticles (USENPs) on HepG2 Carcinoma Cells Resulting from Degradation of Epidermal Growth Factor Receptor (EGFR) with an Evaluation of Its Antiviral and Antioxidant Activities. *Appl. Sci.* **2022**, *12*, 11546. [[CrossRef](#)]
51. Kondaparthi, P.; Flora, S.; Naqvi, S. Selenium nanoparticles: An insight on its Pro-oxidant and antioxidant properties. *Front. Nanosci. Nanotechnol.* **2019**, *6*, 1000189. [[CrossRef](#)]
52. Khurana, A.; Tekula, S.; Saifi, M.A.; Venkatesh, P.; Godugu, C. Therapeutic applications of selenium nanoparticles. *Biomed. Pharmacother.* **2019**, *111*, 802–812. [[CrossRef](#)] [[PubMed](#)]
53. Makvandi, P.; Wang, C.Y.; Zare, E.N.; Borzacchiello, A.; Niu, L.N.; Tay, F.R. Metal-Based Nanomaterials in Biomedical Applications: Antimicrobial Activity and Cytotoxicity Aspects. *Adv. Funct. Mater.* **2020**, *30*, 1910021. [[CrossRef](#)]
54. Hashem, A.H.; Khalil, A.M.A.; Reyad, A.M.; Salem, S.S. Biomedical Applications of Mycosynthesized Selenium Nanoparticles Using *Penicillium expansum* ATTC 36200. *Biol. Trace Element Res.* **2021**, *199*, 3998–4008. [[CrossRef](#)] [[PubMed](#)]
55. Saied, E.; Salem, S.S.; Al-Askar, A.A.; Elkady, F.M.; Arishi, A.A.; Hashem, A.H.J.B. Mycosynthesis of hematite ( $\alpha$ -Fe<sub>2</sub>O<sub>3</sub>) nanoparticles using *Aspergillus niger* and their antimicrobial and photocatalytic activities. *Bioengineering* **2022**, *9*, 397. [[CrossRef](#)]
56. Mohamed, A.A.; Hassan, S.E.-D.; Fouda, A.; Elgamal, M.S.; Salem, S.S. Extracellular Biosynthesis of Silver Nanoparticles Using *Aspergillus* sp. and Evaluation of their Antibacterial and Cytotoxicity. *J. Appl. Life Sci. Int.* **2017**, *11*, 1–12. [[CrossRef](#)]
57. Albalawi, M.A.; Abdelaziz, A.M.; Attia, M.S.; Saied, E.; Elganzory, H.H.; Hashem, A.H.J.A. Mycosynthesis of Silica Nanoparticles Using *Aspergillus niger*: Control of *Alternaria solani* Causing Early Blight Disease, Induction of Innate Immunity and Reducing of Oxidative Stress in Eggplant. *Antioxidants* **2022**, *11*, 2323. [[CrossRef](#)]
58. Fouda, A.; Hassan, S.E.-D.; Saied, E.; Azab, M.S. An eco-friendly approach to textile and tannery wastewater treatment using maghemite nanoparticles ( $\gamma$ -Fe<sub>2</sub>O<sub>3</sub>-NPs) fabricated by *Penicillium expansum* strain (K-w). *J. Environ. Chem. Eng.* **2020**, *9*, 104693. [[CrossRef](#)]
59. Perez, C. Antibiotic assay by agar-well diffusion method. *Acta. Biol. Med. Exp.* **1990**, *15*, 113–115.
60. Bataghva, F.; Sajjadi, S.M.; Daraei, B. Simultaneous Spectrophotometric Quantification of Crystal Violet and Malachite Green in Aqueous Samples: Combination of Multivariate Calibration Method and Solid Phase Extraction Based on Sodium Dodecyl Sulfate (SDS) Grafted Chitosan Nano-composite. *Anal. Bioanal. Chem. Res.* **2020**, *7*, 525–539. [[CrossRef](#)]
61. Saied, E.; Hashem, A.H.; Ali, O.M.; Selim, S.; Almuhayawi, M.S.; Elbahnasawy, M.A. Photocatalytic and Antimicrobial Activities of Biosynthesized Silver Nanoparticles Using *Cytobacillus firmus*. *Life* **2022**, *12*, 1331. [[CrossRef](#)]
62. Bafghi, M.H.; Nazari, R.; Darroudi, M.; Zargar, M.; Zarrinfar, H.J.B.P. The effect of biosynthesized selenium nanoparticles on the expression of CYP51A and HSP90 antifungal resistance genes in *Aspergillus fumigatus* and *Aspergillus flavus*. *Biotechnol. Prog.* **2022**, *38*, e3206. [[CrossRef](#)]
63. Zikalala, N.; Matshetshe, K.; Parani, S.; Oluwafemi, O.S. Biosynthesis protocols for colloidal metal oxide nanoparticles. *Nano-Struct. Nano-Objects* **2018**, *16*, 288–299. [[CrossRef](#)]
64. Khandel, P.; Shahi, S.K. Mycogenic nanoparticles and their bio-prospective applications: Current status and future challenges. *J. Nanostruct. Chem.* **2018**, *8*, 369–391. [[CrossRef](#)]
65. Islam, S.N.; Naqvi, S.M.A.; Raza, A.; Jaiswal, A.; Singh, A.K.; Dixit, M.; Barnwal, A.; Gambhir, S.; Ahmad, A. Mycosynthesis of highly fluorescent selenium nanoparticles from *Fusarium oxysporum*, their antifungal activity against black fungus *Aspergillus niger*, and in-vivo biodistribution studies. *3 Biotech* **2022**, *12*, 1–11. [[CrossRef](#)] [[PubMed](#)]
66. El-Sayed, E.-S.R.; Abdelhakim, H.K.; Ahmed, A.S.J.B. Solid-state fermentation for enhanced production of selenium nanoparticles by gamma-irradiated *Monascus purpureus* and their biological evaluation and photocatalytic activities. *Bioprocess Biosyst. Eng.* **2020**, *43*, 797–809. [[CrossRef](#)]
67. Teeling, E.C.; Springer, M.S.; Madsen, O.; Bates, P.; O'Brien, S.J.; Murphy, W.J. A Molecular Phylogeny for Bats Illuminates Biogeography and the Fossil Record. *Science* **2005**, *307*, 580–584. [[CrossRef](#)] [[PubMed](#)]
68. Saroha, J.; Lalla, N.; Kumar, M.; Sharma, S.N. Ultrafast transient absorption spectroscopic studies on the Impact of growth time on size, stability, and optical characteristics of colloidal gold nanoparticles. *Optik* **2022**, *268*, 169759. [[CrossRef](#)]
69. Hassan, H.U.; Raja, N.I.; Abasi, F.; Mehmood, A.; Qureshi, R.; Manzoor, Z.; Shahbaz, M.; Proćków, J. Comparative Study of Antimicrobial and Antioxidant Potential of *Olea ferruginea* Fruit Extract and Its Mediated Selenium Nanoparticles. *Molecules* **2022**, *27*, 5194. [[CrossRef](#)]
70. Zahra, S.E.; Iqbal, M.S.; Abbas, K.; Qadir, M.I. Synthesis, characterization and evaluation of biological properties of selenium nanoparticles from *Solanum lycopersicum*. *Arab. J. Chem.* **2022**, *15*, 103901. [[CrossRef](#)]
71. Ranjitha, V.; Ravishankar, V.R. Extracellular synthesis of selenium nanoparticles from an actinomycetes streptomyces griseoruber and evaluation of its cytotoxicity on HT-29 cell line. *Pharm. Nanotechnol.* **2018**, *6*, 61–68. [[CrossRef](#)]
72. A Wadhvani, S.; Gorain, M.; Banerjee, P.; Shedbalkar, U.U.; Singh, R.; Kundu, G.C.; A Chopade, B. Green synthesis of selenium nanoparticles using *Acinetobacter* sp. SW30: Optimization, characterization and its anticancer activity in breast cancer cells. *Int. J. Nanomed.* **2017**, *12*, 6841–6855. [[CrossRef](#)]
73. Fouda, A.; Al-Otaibi, W.A.; Saber, T.; AlMotwaa, S.M.; Alshallash, K.S.; Elhady, M.; Badr, N.F.; Abdel-Rahman, M.A. Antimicrobial, antiviral, and in-vitro cytotoxicity and mosquitocidal activities of *Portulaca oleracea*-based green synthesis of selenium nanoparticles. *J. Funct. Biomater.* **2022**, *13*, 157. [[CrossRef](#)]

74. Anmol, A.; Jaiswal, S.K.; Prakash, R.; Mihara, H.; Prakash, N.T. Concomitant synthesis and stabilization of selenium nanoparticles using extract of endophytic fungus, *Nigrospora gullinensis*. *Res. Sq.* **2022**. preprint. [[CrossRef](#)]
75. Arumugham, T.; Alagumuthu, M.; Amimodu, R.G.; Munusamy, S.; Iyer, S.K. A sustainable synthesis of green carbon quantum dot (CQD) from *Catharanthus roseus* (white flowering plant) leaves and investigation of its dual fluorescence responsive behavior in multi-ion detection and biological applications. *Sustain. Mater. Technol.* **2020**, *23*, e00138. [[CrossRef](#)]
76. A Hernández-Díaz, J.; Garza-García, J.J.; León-Morales, J.M.; Zamudio-Ojeda, A.; Arratia-Quijada, J.; Velázquez-Juárez, G.; López-Velázquez, J.C.; García-Morales, S. Antibacterial Activity of Biosynthesized Selenium Nanoparticles Using Extracts of *Calendula officinalis* against Potentially Clinical Bacterial Strains. *Molecules* **2021**, *26*, 5929. [[CrossRef](#)]
77. Qin, L.; Liang, F.; Li, Y.; Wu, J.; Guan, S.; Wu, M.; Xie, S.; Luo, M.; Ma, D. A 2D Porous Zinc-Organic Framework Platform for Loading of 5-Fluorouracil. *Inorganics* **2022**, *10*, 202. [[CrossRef](#)]
78. Qin, L.; Li, Y.; Liang, F.; Li, L.; Lan, Y.; Li, Z.; Lu, X.; Yang, M.; Ma, D. A microporous 2D cobalt-based MOF with pyridyl sites and open metal sites for selective adsorption of CO<sub>2</sub>. *Microporous Mesoporous Mater.* **2022**, *341*, 112098. [[CrossRef](#)]
79. Alam, H.; Khatoun, N.; Khan, M.A.; Husain, S.A.; Saravanan, M.; Sardar, M. Synthesis of Selenium Nanoparticles Using Probiotic Bacteria *Lactobacillus acidophilus* and Their Enhanced Antimicrobial Activity Against Resistant Bacteria. *J. Clust. Sci.* **2019**, *31*, 1003–1011. [[CrossRef](#)]
80. Li, S.; Ren, X.; Mezari, B.; Liu, Y.; Pornsetmetakul, P.; Liutkova, A.; Kosinov, N.; Hensen, E.J. Direct synthesis of Al-rich ZSM-5 nanocrystals with improved catalytic performance in aromatics formation from methane and methanol. *Microporous Mesoporous Mater.* **2023**, *351*, 112485. [[CrossRef](#)]
81. Hassanien, R.; Abed-Elmageed, A.A.I.; Husein, D.Z. Eco-Friendly Approach to Synthesize Selenium Nanoparticles: Photocatalytic Degradation of Sunset Yellow Azo Dye and Anticancer Activity. *Chemistryselect* **2019**, *4*, 9018–9026. [[CrossRef](#)]
82. Al Jahdaly, B.A.; Al-Radadi, N.S.; Eldin, G.M.; Almahri, A.; Ahmed, M.; Shoueir, K.; Janowska, I. Selenium nanoparticles synthesized using an eco-friendly method: Dye decolorization from aqueous solutions, cell viability, antioxidant, and antibacterial effectiveness. *J. Mater. Res. Technol.* **2021**, *11*, 85–97. [[CrossRef](#)]
83. Qian, F.; Li, X.; Tang, L.; Lai, S.K.; Lu, C.; Lau, S.P. Selenium quantum dots: Preparation, structure, and properties. *Appl. Phys. Lett.* **2017**, *110*, 053104. [[CrossRef](#)]
84. Jena, J.; Pradhan, N.; Dash, B.P.; Sukla, L.B.; Panda, P.K. Biosynthesis and characterization of silver nanoparticles using microalga *Chlorococcum humicola* and its antibacterial activity. *Int. J. Nanomater. Biostruct* **2013**, *3*, 1–8.
85. Mekky, A.E.; Farrag, A.A.; Hmed, A.A.; Sofy, A.R. Preparation of Zinc Oxide Nanoparticles using *Aspergillus niger* as Antimicrobial and Anticancer Agents. *J. Pure Appl. Microbiol.* **2021**, *15*, 1547–1566. [[CrossRef](#)]
86. Garza-García, J.J.O.; Hernández-Díaz, J.A.; Zamudio-Ojeda, A.; León-Morales, J.M.; Guerrero-Guzmán, A.; Sánchez-Chiprés, D.R.; López-Velázquez, J.C.; García-Morales, S. The Role of Selenium Nanoparticles in Agriculture and Food Technology. *Biol. Trace Element Res.* **2021**, *200*, 2528–2548. [[CrossRef](#)]
87. Hosnedlova, B.; Kepinska, M.; Skalickova, S.; Fernandez, C.; Ruttkay-Nedecky, B.; Peng, Q.; Kizek, R. Nano-selenium and its nanomedicine applications: A critical review. *Int. J. Nanomed.* **2018**, *13*, 2107–2128. [[CrossRef](#)]
88. Ikram, M.; Javed, B.; Raja, N.I.; Mashwani, Z.-U. Biomedical Potential of Plant-Based Selenium Nanoparticles: A Comprehensive Review on Therapeutic and Mechanistic Aspects. *Int. J. Nanomed.* **2021**, *16*, 249–268. [[CrossRef](#)]
89. Muthu, S.; Raju, V.; Gopal, V.B.; Gunasekaran, A.; Narayan, K.S.; Malairaj, S.; Lakshmikanthan, M.; Duraisamy, N.; Krishnan, K.; Perumal, P. A rapid synthesis and antibacterial property of selenium nanoparticles using egg white lysozyme as a stabilizing agent. *SN Appl. Sci.* **2019**, *1*, 1543. [[CrossRef](#)]
90. Shubharani, R.; Mahesh, M.; Yogananda Murthy, V. Biosynthesis and characterization, antioxidant and antimicrobial activities of selenium nanoparticles from ethanol extract of Bee Propolis. *J. Nanomed. Nanotechnol.* **2019**, *10*, 1000522.
91. Hernández-Díaz, J.A.; Garza-García, J.J.; Zamudio-Ojeda, A.; León-Morales, J.M.; López-Velázquez, J.C.; García-Morales, S. Plant-mediated synthesis of nanoparticles and their antimicrobial activity against phytopathogens. *J. Sci. Food Agric.* **2021**, *101*, 1270–1287. [[CrossRef](#)]
92. Zafar, M.N.; Dar, Q.; Nawaz, F.; Zafar, M.N.; Iqbal, M.; Nazar, M.F. Effective adsorptive removal of azo dyes over spherical ZnO nanoparticles. *J. Mater. Res. Technol.* **2019**, *8*, 713–725. [[CrossRef](#)]
93. Bayram, O.; Köksal, E.; Moral, E.; Göde, F.; Pehlivan, E. Efficient decolorization of cationic dye (malachite green) by natural-based biosorbent (nano-magnetic *Sophora Japonica* fruit seed biochar). *J. Dispers. Sci. Technol.* **2022**, 1–12. [[CrossRef](#)]
94. Cittrarasu, V.; Kaliannan, D.; Dharman, K.; Maluventhen, V.; Easwaran, M.; Liu, W.C.; Balasubramanian, B.; Arumugam, M. Green synthesis of selenium nanoparticles mediated from *Ceropegia bulbosa* Roxb extract and its cytotoxicity, antimicrobial, mosquitocidal and photocatalytic activities. *Sci. Rep.* **2021**, *11*, 1032. [[CrossRef](#)]
95. Akinola, P.; Lateef, A.; Asafa, T.; Beukes, L.; Hakeem, A.; Irshad, H. Multifunctional titanium dioxide nanoparticles biofabricated via photosynthetic route using extracts of *Cola nitida*: Antimicrobial, dye degradation, antioxidant and anticoagulant activities. *Heliyon* **2020**, *6*, e04610. [[CrossRef](#)] [[PubMed](#)]
96. El-Naggar, M.E.; Shoueir, K. Recent advances in polymer/metal/metal oxide hybrid nanostructures for catalytic applications: A review. *J. Environ. Chem. Eng.* **2020**, *8*, 104175.
97. Sackey, J.; Bashir, A.; Ameh, A.; Nkosi, M.; Kaonga, C.; Maaza, M. Date pits extracts assisted synthesis of magnesium oxides nanoparticles and its application towards the photocatalytic degradation of methylene blue. *J. King Saud Univ. Sci.* **2020**, *32*, 2767–2776. [[CrossRef](#)]

98. Bhadra, J.; Parangusan, H.; Popelka, A.; Lehocky, M.; Humpolicek, P.; Al-Thani, N. Electrospun Polystyrene/PANI-Ag fibers for organic dye removal and antibacterial application. *J. Environ. Chem. Eng.* **2020**, *8*, 103746. [[CrossRef](#)]
99. Neves, T.D.F.; Dalarme, N.B.; da Silva, P.M.M.; Landers, R.; Picone, C.S.F.; Prediger, P. Novel magnetic chitosan/quaternary ammonium salt graphene oxide composite applied to dye removal. *J. Environ. Chem. Eng.* **2020**, *8*, 103820. [[CrossRef](#)]
100. Wang, J.; Liu, J.; Du, Z.; Li, Z. Recent advances in metal halide perovskite photocatalysts: Properties, synthesis and applications. *J. Energy Chem.* **2020**, *54*, 770–785. [[CrossRef](#)]

**Disclaimer/Publisher's Note:** The statements, opinions and data contained in all publications are solely those of the individual author(s) and contributor(s) and not of MDPI and/or the editor(s). MDPI and/or the editor(s) disclaim responsibility for any injury to people or property resulting from any ideas, methods, instructions or products referred to in the content.